Thermochimica Acta 503–504 (2010) 100–107

Contents lists available at ScienceDirect

Thermochimica Acta

journal homepage: www.elsevier.com/locate/tca

Measurement of specific heat and specific absorption rate by nuclear magnetic resonance

David H. Gultekin[a,b,c,h,*], John C. Gore[d,e,f,g,h]

[a] Department of Electrical Engineering, Yale University, New Haven, CT 06520, USA
[b] Department of Medical Physics, Memorial Sloan-Kettering Cancer Center, New York, NY 10065 USA
[c] Department of Radiology, Memorial Sloan-Kettering Cancer Center, New York, NY 10065 USA
[d] Department of Biomedical Engineering, Vanderbilt University, Nashville, TN 37232 USA
[e] Department of Radiology and Radiological Sciences, Vanderbilt University, Nashville, TN 37232 USA
[f] Department of Molecular Physiology and Biophysics, Vanderbilt University, Nashville, TN 37232 USA
[g] Department of Physics and Astronomy, Vanderbilt University, Nashville, TN 37232 USA
[h] Institute of Imaging Science, Vanderbilt University, Nashville, TN 37232 USA

ARTICLE INFO

Article history:
Received 28 October 2009
Received in revised form 3 March 2010
Accepted 17 March 2010
Available online 25 March 2010

Keywords:
NMR calorimetry
Specific heat
Specific absorption rate
Temperature
Absorptance

ABSTRACT

We evaluate a nuclear magnetic resonance (NMR) method of calorimetry for the measurement of specific heat (c_p) and specific absorption rate (SAR) in liquids. The feasibility of NMR calorimetry is demonstrated by experimental measurements of water, ethylene glycol and glycerol using any of three different NMR parameters (chemical shift, spin–spin relaxation rate and equilibrium nuclear magnetization). The method involves heating the sample using a continuous wave laser beam and measuring the temporal variation of the spatially averaged NMR parameter by non-invasive means. The temporal variation of the spatially averaged NMR parameter as a function of thermal power yields the ratio of the heat capacity to the respective nuclear thermal coefficient, from which the specific heat can be determined for the substance. The specific absorption rate is obtained by subjecting the liquid to heating by two types of radiation, radiofrequency (RF) and near-infrared (NIR), and by measuring the change in the nuclear spin phase shift by a gradient echo imaging sequence. These studies suggest NMR may be a useful tool for measurements of the thermal properties of liquids.

1. Introduction

Knowledge of the thermophysical properties of substances is important in many fields including thermodynamics, materials science, food science, engineering, chemistry, biology and medicine. The study of the interaction of thermal energy with materials, and quantifying the relationship between the thermal energy and the temperature, is known as calorimetry. Calorimetry has been used for the thermal characterization of substances in various fields including thermophysics and thermochemistry [1,2], polymer science [3], food science [4], pharmaceutical science [5] and structural biology [6].

The specific heat of a substance determines the resulting temperature change in a unit quantity of the substance for a given amount of heat input or output [7]. Specific heat can be measured by several different methods [1,2,8] but two main approaches are commonly used, differential scanning calorimetry (DSC) [9] and modulated temperature differential scanning calorimetry (MTDSC) [10,11]. Over the years, there have been significant improvements in DSC and its variations leading to high accuracy and a wide range of applications. However, the basic principle by which a sample is measured in a pan using a contact temperature and a reference has remained the same [12–14]. A method for measuring the specific heat (c_p) and specific absorption rate (SAR) of a material non-invasively and remotely throughout the volume could have significant advantages over current approaches in some applications.

Here we demonstrate how NMR may be used to measure the thermal properties of liquids by measuring the temporal variation of NMR parameters in the sample after heating by an external source. The temporal variation of NMR parameters as a function of thermal power yields the ratio of the heat capacity to the respective nuclear thermal coefficient from which the specific heat can be determined experimentally for the substance [15].

The specific absorption rate (SAR) produced by radiofrequency (RF) heating can in principle be calculated for substances from knowing the electrical conductivity and the electric field, but in practice these estimates are difficult. Analytical electromagnetic solutions [16], electromagnetic modelling [17,18] and thermal

* Corresponding author at: Memorial Sloan-Kettering Cancer Center, 1275 York Avenue, New York, NY 10065, USA. Tel.: +1 212 639 7359.
E-mail address: david.gultekin@aya.yale.edu (D.H. Gultekin).

0040-6031/$ – see front matter © 2010 Elsevier B.V. All rights reserved.
doi:10.1016/j.tca.2010.03.015

measurements [19] have each been used to predict or estimate SAR. SAR in general varies spatially and temporally but SAR is usually averaged over a specified mass and time during exposure to devices such as wireless phones [20,21] and diagnostic magnetic resonance imaging equipment [22–24]. A calorimetric method, as proposed here, may provide a direct measurement of the SAR in substances. However, estimation of SAR experimentally requires the measurement of, or the prior knowledge of, the specific heat of the substance [15]. Here, we measure SAR by subjecting a sample to electromagnetic radiation in a transparent cell and measuring the temporal variation of NMR parameters. The experimental SAR value is then calculated using the ratio of the specific heat to the respective nuclear thermal coefficient.

2. Theory

2.1. Specific heat

The method described here involves application of heat to a sample volume and the measurement of the temporal variation of a spatially averaged NMR parameter within this volume. The thermal energy change in this volume will result in a temperature change within the volume

$$dQ = \left(\frac{\partial Q}{\partial T}\right) dT \tag{1}$$

Over a narrow temperature range (few K), the temperature dependence of thermal energy in the substance can be taken as constant, and the integration of this equation over a time interval from 0 to t yields

$$Q(t) = Q(0) - T(0)\left(\frac{\partial Q}{\partial T}\right) + T(t)\left(\frac{\partial Q}{\partial T}\right) \tag{2}$$

for the amount of heat in the substance as a function of time. Taking the first order temporal derivative of Eq. (2) as

$$\frac{\partial Q(t)}{\partial t} = \left(\frac{\partial Q}{\partial T}\right)\frac{\partial T(t)}{\partial t} \tag{3}$$

we find a relation between the temporal variations of thermal energy and temperature.

Several NMR parameters are sensitive to temperature, and for our purposes we have evaluated three of these. Using the linear relation between the dimensionless nuclear shielding [25–28] and temperature, and the relation of Eq. (1), and integrating it over a range of time from 0 to t and taking the temporal derivative of it yields

$$\frac{\partial \sigma(t)}{\partial t} = \left(\frac{\partial \sigma}{\partial T}\right)\frac{\partial T(t)}{\partial t} \tag{4}$$

Substituting Eq. (4) into Eq. (3), the temporal variation of thermal energy in the substance can be written as

$$\frac{\partial Q(t)}{\partial t} = \left(\frac{\partial Q}{\partial T}\right)\left(\frac{\partial \sigma}{\partial T}\right)^{-1}\frac{\partial \sigma(t)}{\partial t} \tag{5}$$

in terms of the temporal variation of nuclear shielding in the substance.

Similarly, the spin–spin relaxation rate (R_2) can be used to monitor the temporal variation of thermal energy in a substance [29,30]. We define a dimensionless spin–spin relaxation rate as

$$\Omega(t) = \frac{R_2(t)}{R_2(0)} \tag{6}$$

where $R_2(0)$ corresponds to time 0 and $R_2(t)$ varies with temperature and time as $T = T(t)$. Using the relation in Eqs. (1) and (6) and taking the temporal derivative of it as

$$\frac{\partial \Omega(t)}{\partial t} = \left(\frac{\partial \Omega}{\partial T}\right)\frac{\partial T(t)}{\partial t} \tag{7}$$

substituting Eq. (7) into Eq. (3), we get the temporal variation of thermal energy as

$$\frac{\partial Q(t)}{\partial t} = \left(\frac{\partial Q}{\partial T}\right)\left(\frac{\partial \Omega}{\partial T}\right)^{-1}\frac{\partial \Omega(t)}{\partial t} \tag{8}$$

in terms of the temporal variation of dimensionless spin–spin relaxation rate.

The energy change in the substance can also be monitored through the measurement of equilibrium nuclear magnetization as

$$M(0,T) = \frac{N\gamma^2\hbar^2 I(I+1)B_0}{3k_B T} \tag{9}$$

where N is the number of spins, γ is the gyromagnetic ratio, $\hbar$ is the angular Planck's constant, I is the spin quantum number, B_0 is the magnetic field, k_B is Boltzmann's constant and T is the absolute temperature [31–34].

We can define a dimensionless equilibrium nuclear magnetization in terms of the dimensionless temperature as

$$M(t) = \frac{M(0,T)}{M(t,T)} = \frac{T(t)}{T(0)} \tag{10}$$

Taking the first order temporal derivative of Eq. (10) as

$$\frac{\partial M(t)}{\partial t} = \left(\frac{\partial M}{\partial T}\right)\frac{\partial T(t)}{\partial t} \tag{11}$$

and substituting Eq. (11) into Eq. (3), we get

$$\frac{\partial Q(t)}{\partial t} = \left(\frac{\partial Q}{\partial T}\right)\left(\frac{\partial M}{\partial T}\right)^{-1}\frac{\partial M(t)}{\partial t} \tag{12}$$

When acquiring an echo signal in NMR, the nuclear shielding can be measured by changes in the nuclear spin phase shift. The spin phase shift for a given nucleus can be formulated as

$$\phi(t) = \gamma \cdot (1 - \sigma(t))B_0 \cdot T_E \tag{13}$$

where γ and B_0 are as before, T_E is the echo time and $\sigma(t)$ is the nuclear shielding varying with time and temperature as $T = T(t)$. Thus, in MR imaging, the temporal variation of nuclear shielding can be measured as

$$\frac{\partial \sigma(t)}{\partial t} = -\frac{1}{\gamma B_0 T_E}\left(\frac{\partial \phi(t)}{\partial t}\right) \tag{14}$$

and its temperature dependence as

$$\left(\frac{\partial \sigma}{\partial T}\right)^{-1} = -\gamma B_0 T_E\left(\frac{\partial \phi}{\partial T}\right)^{-1} \tag{15}$$

Substituting Eqs. (14) and (15) into Eq. (5), we get

$$\frac{\partial Q(t)}{\partial t} = \left(\frac{\partial Q}{\partial T}\right)\left(\frac{\partial \phi}{\partial T}\right)^{-1}\frac{\partial \phi(t)}{\partial t} \tag{16}$$

in terms of temperature dependence and temporal variation of nuclear spin phase shift.

The experimental temperature dependent and time dependent parameters along with their units are given in Table 1.

The parameter C_T is the heat capacity or the thermal mass of the substance. The parameters σ_T, Ω_T, M_T and ϕ_T, here referred to as the nuclear thermal coefficients, are specific to each substance and can be determined experimentally by measuring the thermally induced changes in these parameters as a function of the temperature [35].

Table 1
Experimental temperature and time dependent parameters along with their units.

Temperature dependent parameters		Time dependent parameters	
Parameters	Units	Parameters	Units
$C_T = \left(\frac{\partial Q}{\partial T}\right)$	$J K^{-1}$	$\dot{Q} = \left(\frac{\partial Q(t)}{\partial t}\right)$	$J s^{-1}$
$\sigma_T = \left(\frac{\partial \sigma}{\partial T}\right)$	K^{-1}	$\dot{\sigma} = \left(\frac{\partial \sigma(t)}{\partial t}\right)$	s^{-1}
$\Omega_T = \left(\frac{\partial \Omega}{\partial T}\right)$	K^{-1}	$\dot{\Omega} = \left(\frac{\partial \Omega(t)}{\partial t}\right)$	s^{-1}
$M_T = \left(\frac{\partial M}{\partial T}\right)$	K^{-1}	$\dot{M} = \left(\frac{\partial M(t)}{\partial t}\right)$	s^{-1}
$\phi_T = \left(\frac{\partial \phi}{\partial T}\right)$	$r K^{-1}$	$\dot{\phi} = \left(\frac{\partial \phi(t)}{\partial t}\right)$	$r s^{-1}$

The parameter $\dot{Q}$ is the rate of energy transfer or power, and $\dot{\sigma}$, $\dot{\Omega}$, $\dot{M}$ and $\dot{\phi}$ are the rates of change in respective NMR parameters.

Per Eq. (15) and Table 1, the nuclear thermal coefficients for spin phase shift and nuclear shielding are related through the following relation

$$\phi_T = -\gamma \cdot B_0 \cdot T_E \cdot \sigma_T \tag{17}$$

and are used in imaging interchangeably.

Applying a constant rate of heating (thermal power) and assuming the heat capacity is a weak function of the temperature over a narrow temperature range (few K), Eqs. (5), (8), (12) and (16) can be written as

$$\frac{\partial Q(t)}{\partial t} = \frac{C_T}{\sigma_T}\frac{\partial \sigma(t)}{\partial t} = \frac{C_T}{\Omega_T}\frac{\partial \Omega(t)}{\partial t} = \frac{C_T}{M_T}\frac{\partial M(t)}{\partial t} = \frac{C_T}{\phi_T}\frac{\partial \phi(t)}{\partial t} \tag{18}$$

or further as

$$\dot{Q} = \frac{C_T}{\sigma_T}\dot{\sigma} = \frac{C_T}{\Omega_T}\dot{\Omega} = \frac{C_T}{M_T}\dot{M} = \frac{C_T}{\phi_T}\dot{\phi} \tag{19}$$

in terms of the temporal variation of the nuclear shielding, dimensionless spin–spin relaxation rate, the dimensionless equilibrium nuclear magnetization and spin phase shift and the ratio of the heat capacity to respective nuclear thermal coefficients, respectively.

A plot of $\dot{Q}$ vs. $\dot{\sigma}$, $\dot{\Omega}$, $\dot{M}$ or $\dot{\phi}$ will yield lines with slopes equal to C_T/σ_T, C_T/Ω_T, C_T/M_T or C_T/ϕ_T, the ratios of the heat capacities to the respective nuclear thermal coefficients, respectively.

The specific heat (c_p) represents the dependence of the heat capacity (C_T) on the mass and can be calculated as

$$c_p = \frac{\partial C_T}{\partial m} = \frac{1}{m}\left(\frac{\partial Q}{\partial T}\right)_p = \frac{1}{\rho V}\left(\frac{\partial Q}{\partial T}\right)_p \tag{20}$$

where m, ρ, and V are the mass, the density and the volume of the sample under constant pressure (p), respectively.

Using Eq. (18), the thermal power can be formulated as

$$P = \frac{C_T}{\phi_T}\frac{d\phi(t)}{dt} \tag{21}$$

and related to the rate of nuclear spin phase shift change and the ratio of the heat capacity to the nuclear thermal coefficient. Further, by expressing the thermal power (P) as a fraction of the incident laser power (P_0) through $P = P_0 A$, and normalizing it for the volume fraction, we have

$$P_0 = \frac{C_T}{\phi_T}\frac{R}{A}\frac{d\phi(t)}{dt} \tag{22}$$

where A is the absorptance for the sample at the corresponding wavelength and R is the ratio of the measurement (imaging) volume to the heating volume.

A plot of P_0 vs. $\dot{\phi}$ yields a slope equal to $C_T R/\phi_T A$, proportional to the ratio of the heat capacity to the nuclear thermal coefficient (C_T/ϕ_T) through the ratio R/A.

2.2. Specific absorption rate

The specific absorption rate (SAR) can also be measured experimentally through the measurement of specific heat and the rate of temperature rise in a substance subjected to electromagnetic radiation. SAR can be expressed as

$$\mathrm{SAR} = \frac{\partial}{\partial m}\left(\frac{\partial Q(t)}{\partial t}\right) = \frac{\partial}{\partial m}\left(\frac{\partial Q}{\partial T}\right)\frac{\partial T(t)}{\partial t} = \frac{\partial C_T}{\partial m}\frac{\partial T(t)}{\partial t} \tag{23}$$

The rate of temperature change is related to the rate of change in the NMR parameters through the respective nuclear thermal coefficients as

$$\frac{dT(t)}{dt} = \frac{1}{\sigma_T}\frac{\partial \sigma(t)}{\partial t} = \frac{1}{\Omega_T}\frac{\partial \Omega(t)}{\partial t} = \frac{1}{M_T}\frac{\partial M(t)}{\partial t} = \frac{1}{\phi_T}\frac{d\phi(t)}{dt} \tag{24}$$

Using Eqs. (20), (23) and (24), SAR for any imaging voxel can then be written as

$$[\mathrm{SAR}]_{i,j,k} = \frac{c_p}{\phi_T}\left[\frac{\partial \phi(t)}{\partial t}\right]_{i,j,k} \tag{25}$$

in terms of the ratio of the specific heat to the nuclear thermal coefficient (c_p/ϕ_T), and the temporal variation of spin phase shift ($\dot{\phi}$) in a voxel corresponding to location (i,j,k) in a Cartesian coordinate system.

NMR calorimetry can be used for measuring the absorbed thermal power (P) in an experiment and from this the absorptance (A) can be estimated for a continuous wave (CW) irradiation. We define the specific incident energy rate (SIR) as the ratio of the irradiating incident power to the mass. SAR is proportional to SIR through A as below.

$$\mathrm{SAR} = \frac{\partial P}{\partial m} = A\frac{\partial P_0}{\partial m} = A \cdot \mathrm{SIR} \tag{26}$$

A plot of P vs. P_0 or a plot of SAR vs. SIR yields a line with its slope equal to A.

3. Experimental methods

As a demonstration of NMR calorimetry, three liquids, water (H_2O), ethylene glycol ($C_2H_4(OH)_2$) and glycerol ($C_3H_5(OH)_3$) were subjected to variable rates of heating by a continuous wave (CW) laser beam in a 2 T magnet. The temporal variations of three NMR parameters, the nuclear shielding, spin–spin relaxation rate and the equilibrium nuclear magnetization, were measured by interleaved spectrometry and relaxometry sequences. The proton chemical shift was measured using a single B_1 pulse followed by a Fourier transform of the free induction decay (FID). The spin-spin relaxation rate and the equilibrium nuclear magnetization were measured by a multi-echo Carr–Purcell–Meiboom–Gill (CPMG) sequence [36,37] using 256 echoes spaced by 0.242–5.0 ms. The echo data were fit to a single exponential decay constant and the curve was extrapolated back to $t = 0$ to obtain the equilibrium magnetization. SAR was measured in a water sample by subjecting it to electromagnetic heating by two means, radiofrequency (RF) and near-infrared (NIR) irradiations, using an NMR transmitter coil and a diode laser, respectively. An interleaved spoiled Gradient Echo (GRE) sequence [38] and a single shot rapid acquisition with relaxation enhancement (RARE) sequence [39] were used for the SAR measurements. The GRE sequence was used to measure the nuclear spin phase shift and the single shot RARE sequence was used to assess RF power deposition. The GRE was used in a coronal plane along the temperature gradients to measure average c_p and in an axial plane to measure local SAR.

To induce heating of the samples, a 15 W CW diode laser (wavelength: 810 nm) was used. The water, ethylene glycol and glycerol are highly transparent to the laser at the wavelength of 810 nm and

Table 2
The rates of change of dimensionless parameters and the temperature (calculated from nuclear shielding) as functions of applied power for water, ethylene glycol and glycerol.

Parameter	Substance	$\dot{Q}$ [W]			
		0.080	0.160	0.240	0.320
$\dot{\sigma}$ [$\times 10^9\ s^{-1}$]	H_2O	−0.0253	−0.0588	−0.0957	−0.1366
	$C_2H_4(OH)_2$	−0.0289	−0.0810	−0.1339	−0.1931
	$C_3H_5(OH)_3$	−0.0623	−0.1246	−0.1784	−0.2333
$\dot{\Omega}$ [$\times 10^3\ s^{-1}$]	H_2O	−0.0236	−0.0581	−0.0893	−0.1220
	$C_2H_4(OH)_2$	−0.1003	−0.2134	−0.3110	−0.4750
	$C_3H_5(OH)_3$	−0.3517	−0.6315	−0.8923	−1.1474
$\dot{M}$ [$\times 10^4\ s^{-1}$]	H_2O	0.0587	0.2048	0.3020	0.4383
	$C_2H_4(OH)_2$	0.1255	0.3479	0.5526	0.7349
	$C_3H_5(OH)_3$	0.0751	0.2388	0.3873	0.5919
$\dot{T}$ [$\times 10^2\ K\,s^{-1}$]	H_2O	0.1708	0.5961	0.8788	1.2753
	$C_2H_4(OH)_2$	0.3653	1.0122	1.6080	2.1387
	$C_3H_5(OH)_3$	0.2187	0.6948	1.1271	1.7225

therefore a common absorber, in this case an electronic grade silicon wafer, was used to absorb the laser light and provide a constant flux of thermal energy. The absorptance (A) of the silicon wafer was measured optically. The laser beam was aimed at the matte finished surface in contact with the liquids. The absorber was removed to measure the SAR of NIR radiation in water and the laser beam was directly aimed into the water using an optical fiber.

Samples of water, ethylene glycol and glycerol in cylindrical cells (ID = 11.3 mm, L =50 mm, V = 5 ml) with their axes aligned with the direction of the B_0 field were subjected to heating using the laser beam with variable incident laser power levels of 0.5, 1.0, 1.5 and 2.0 W corresponding to thermal powers of 80, 160, 240 and 320 mW through a common absorber (A = 0.16) in the calorimeter cells. In each experiment, the laser power was maintained constant and the temperature of the sample was allowed to change over the experimental time. The cells were thermally insulated to minimize the heat loss from the samples to the environment.

The subsequent temporal and spatial variations of changes in the NMR parameters were monitored using a 2 T Bruker NMR System (Bruker Biospin, USA). The spectroscopic parameters were, pulse length (t_p) 100 μs, bandwidth (BW) 2 kHz, number of points (N) 8192, spectral resolution (Hz) 0.1 Hz, birdcage resonator ID = 72 mm. The CPMG parameters were; echo time (T_E) 0.242–5.0 ms, number of echoes (n) 256, bandwidth (BW) 1 kHz, repetition time (T_R) 23 s. The GRE imaging parameters were; BW = 16 kHz, T_E = 11 ms, T_R = 90 ms, matrix size (m) 128 × 128, field of view (FOV) 64 mm (coronal) and 35 mm (axial), slice thickness (z) 4 mm (coronal) and 3 mm (axial), flip angle (θ) $\pi/4$, and number of excitations (NEX) 1, number of experiments (N_E) 30. The RARE sequence parameters were; single shot RARE, rare factor (RF) or number of pulses (n_p) 128, m = 128 × 128, refocusing pulse length (t_p) 2 ms and $\theta = \pi$, T_E = 15.6 ms, T_R = 23 s, FOV = 30 mm, BW = 35 kHz and NEX = 1. The pulse power (P_p) was estimated as 2.5 W using maximum RF amplifier power of 1000 W and the attenuation of 26 dB. The duty cycles for pulse sequence ($D_1 = t_p/T_E$) and pulse sequence repetition ($D_2 = t_p n_p/T_R$) were 0.128 and 0.011, respectively. The average RF powers for pulse sequence ($P_1 = P_p D_1$) and pulse sequence repetition ($P_2 = P_p D_2$) were 0.32 and 0.0275 W, respectively. The ParaVision software (Bruker BioSpin, USA) and Matlab software (Mathworks, USA) were used for the analysis of the experimental data.

4. Results and discussion

The thermally induced temporal variations of spatially averaged nuclear shielding, dimensionless spin–spin relaxation rate and the dimensionless equilibrium nuclear magnetization, are given in Fig. 1 as functions of incident laser power following the application of the laser energy at t = 0 s.

Table 3
Nuclear thermal coefficients (σ_T, Ω_T and M_T) and slopes of lines (C_T/σ_T, C_T/Ω_T and C_T/M_T) for water, ethylene glycol and glycerol.

Parameter	H_2O	$C_2H_4(OH)_2$	$C_3H_5(OH)_3$
σ_T [$\times 10^7\ K^{-1}$]	−0.10	−0.09	−0.11
Ω_T [$\times 10^1\ K^{-1}$]	−0.0950	−0.2170	−0.5010
M_T [$\times 10^3\ K^{-1}$]	3.4364	3.4364	3.4364
$\frac{C_T}{\sigma_T}$ [$\times 10^{-9}$ J]	−2.1537	−1.4654	−1.4098
$\frac{C_T}{\Omega_T}$ [$\times 10^{-3}$ J]	−2.4510	−0.6463	−0.3020
$\frac{C_T}{M_T}$ [$\times 10^{-3}$ J]	6.4386	3.9276	4.6870

A linear regression of the dimensionless NMR parameters vs. time in Fig. 1 yields the rates of these parameters as functions of the thermal power and are given in Table 2. The heating rates ($\dot{T}$) as measured through the nuclear shielding in substances are given as functions of laser power levels ($\dot{Q}$) in the bottom row of Table 2.

A plot of $\dot{Q}$ vs. $\dot{\sigma}$, $\dot{\Omega}$ and $\dot{M}$ yields lines with slopes equal to C_T/σ_T, C_T/Ω_T and C_T/M_T, the ratios of the heat capacities to the respective nuclear thermal coefficients, for H_2O, $C_2H_4(OH)_2$ and $C_3H_5(OH)_3$ as given in Fig. 2. The slopes of lines in Fig. 2 simply yield the amount of thermal energy in the units of Joules per unit changes in the respective dimensionless NMR parameters.

The experimental nuclear thermal coefficients and the slopes of lines shown in Fig. 2 for water, ethylene glycol and glycerol are given in Table 3.

The density, volume, mass, specific heat and heat capacity for water, ethylene glycol and glycerol at room temperature and atmospheric pressure are given in Table 4.

Using the experimental data in Tables 3 and 4 and Eq. (20), the specific heat can be calculated for the liquids. The specific heat of water, ethylene glycol and glycerol as measured by three different NMR parameters are given in Table 5.

Table 4
The experimental and reference parameters for water, ethylene glycol and glycerol at room temperature and atmospheric pressure.

	H_2O	$C_2H_4(OH)_2$	$C_3H_5(OH)_3$
ρ [$\times 10^{-3}$ kg m^{-3}][a]	0.998	1.113	1.261
V [$\times 10^6$ m^3][a]	5.0	5.0	5.0
m [$\times 10^3$ kg][a]	4.991	5.566	6.305
c_p [$\times 10^{-3}$ J kg^{-1} K^{-1}][b]	4.186	2.380	2.360
C_T [$\times 10^{-2}$ J K^{-1}][c]	0.2089	0.1325	0.1488

[a] Measured.
[b] Reference.
[c] Calculated.

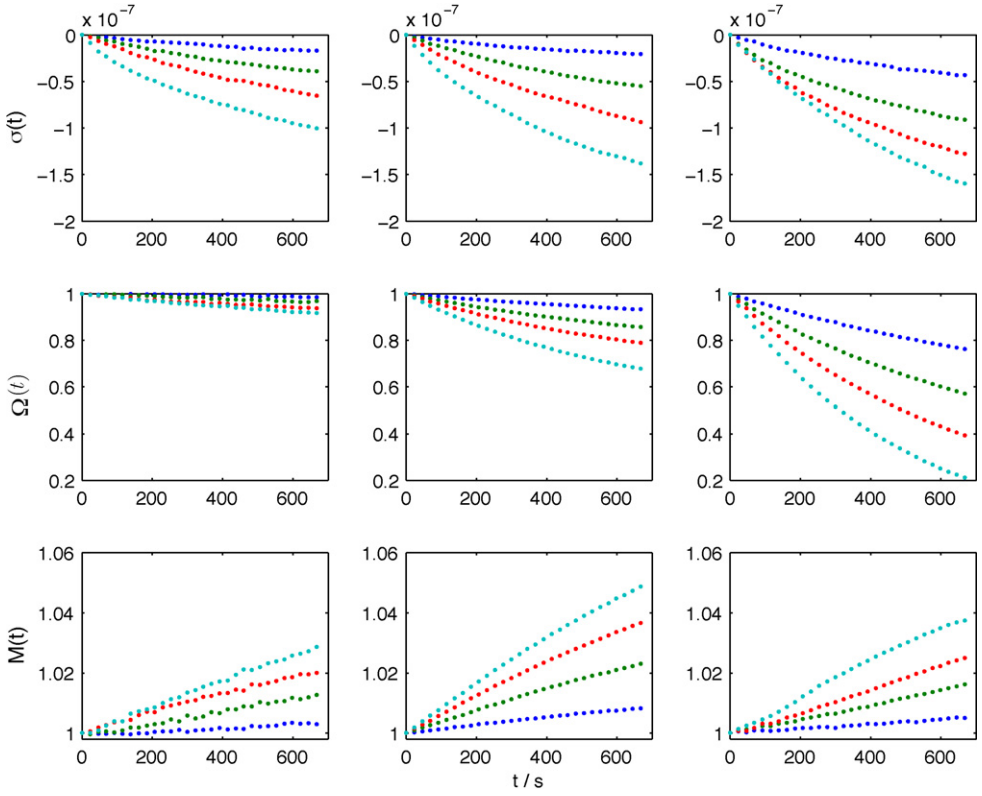

Fig. 1. Experimental variation of dimensionless σ (top), Ω (middle) and M (bottom) rows as a function of time and laser power (0.08, 0.16, 0.24 and 0.32 W corresponding to curves in increasing/decreasing order) for water (left), ethylene glycol (middle) and glycerol (right) columns.

The experimental nuclear spin phase shift vs. time for a water sample subjected to different levels of Thermal and NIR powers are given in Fig. 3. A coronal imaging plane (z = 4 mm) along the direction of temperature gradient is used to measure average c_p in water subjected to 0.08, 0.16, 0.24 and 0.32 W thermal power (a). An axial plane (z = 3 mm) is used to measure local SAR in 0.3 g of water in the center of a cylindrical cell (ID = 11.3 mm, L = 50 mm) subjected to 1, 2, 3 and 4 W NIR laser power delivered through an optical fiber along the axis (b). Plots of P_0 vs. $\dot{\phi}$ and SAR vs. SIR yield slopes (s) of $C_T R/\phi_T A$ and A, respectively (c and d).

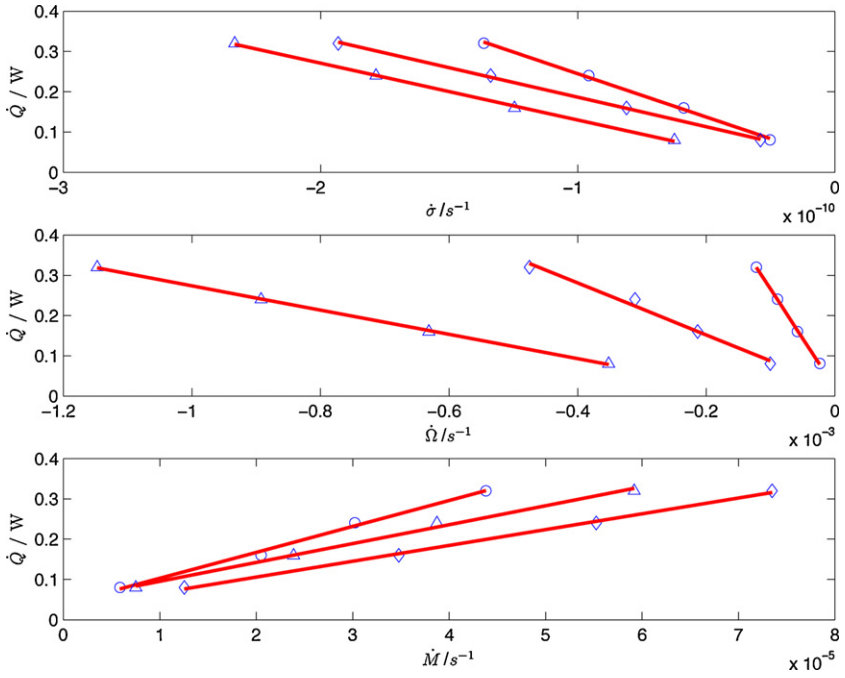

Fig. 2. Experimental plot of $\dot{Q}$ vs. $\dot{\sigma}$ (top), $\dot{\Omega}$ (middle) and $\dot{M}$ (bottom) for water (○), ethylene glycol (◊) and glycerol (△). The open legends are experimental data and the solid red lines are fitted functions to the data. The slopes equal to the ratios of the heat capacities to the nuclear thermal coefficients for each substance. (For interpretation of the references to color in this figure legend, the reader is referred to the web version of the article.)

Table 5
Experimental specific heat for H_2O, $C_2H_4(OH)_2$ and $C_3H_5(OH)_3$ as measured by three different NMR parameters at a 2 T magnet.

Specific heat [J kg^{-1} K^{-1}]	NMR parameter [dimensionless]	Water (H_2O)	Ethylene glycol ($C_2H_4(OH)_2$)	Glycerol ($C_3H_5(OH)_3$)
c_p	$\sigma(t)$	4315	2369	2459
c_p	$\Omega(t)$	4672	2516	2401
c_p	$M(t)$	4433	2424	2554

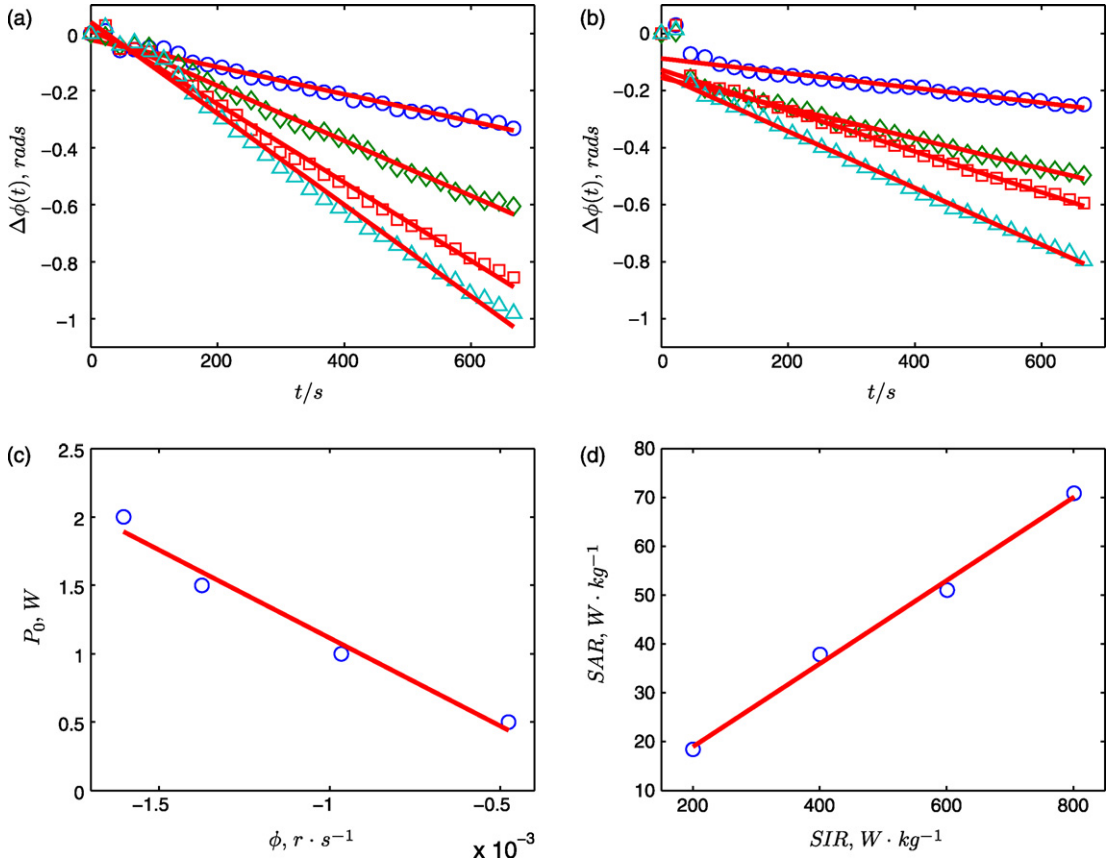

Fig. 3. Experimental nuclear spin phase shift ($\Delta\phi$) measured by a GRE sequence vs. time for a water sample subjected to 0.08, 0.16, 0.24 and 0.32 W thermal powers (a) and 1, 2, 3 and 4 W NIR laser powers (b) at a 2 T magnet. Plots of P_0 vs. $\dot{\phi}$ (c) and SAR vs. SIR (d) have slopes (s) of $C_T R/\phi_T A$ and A, respectively. The open legends are experimental data and the solid red lines are fitted functions to the data. (For interpretation of the references to color in this figure legend, the reader is referred to the web version of the article.)

Substituting the experimental parameters into Eq. (17) and calculating the nuclear thermal coefficient for the spin phase shift as

$$\phi_T = -\gamma \cdot B_0 \cdot T_E \cdot \sigma_T = -0.05885 \text{ r K}^{-1} \quad (27)$$

and using the slope ($s = -1287.6$ J r^{-1}) in Fig. 3(c) and the volume ratio of $R = 1/1.9$ per Eq. (22), the specific heat can be calculated for water as 4616 J kg^{-1} K^{-1} vs. the literature value of 4186 J kg^{-1} K^{-1} at 295 K (Table 4) and 4315 J kg^{-1} K^{-1} as measured by the nuclear shielding method (Table 5).

The measurement of SAR by thermal methods requires the knowledge of c_p in substances. The ability to measure c_p by NMR calorimetry provides means for the measurement of local SAR with a high temporal and spatial resolution. SAR varies spatially and temporally which requires specification of SAR over space and time.

The experimental spatial and temporal variation of nuclear spin phase shift ($\dot{\phi}$), temperature ($\dot{\phi}/\phi_T$), and specific absorption rate ($c_p\dot{\phi}/\phi_T$) measured by a GRE imaging sequence in 0.3 g of water sample subjected to NIR laser powers at a 2 T magnet are given in Fig. 4.

Using the slopes of lines ($\dot{\phi}$) corresponding to thermal power in Fig. 3(a) and Eq. (22), the specific heat of water can be calculated, and using Eq. (25), SAR can be estimated for NIR and RF radiation in water as given in Table 6.

The spatial and temporal variation of SAR (averaged over 5, 10 and 12 min) in 0.3 g of water in a 3 mm axial GRE imaging slice in the center of a cylindrical cell (ID = 11.3 mm, L = 50 mm) as functions of NIR laser irradiation powers of 1, 2, 3 and 4 W are visualized in Fig. 5.

Using the ratio of the heat capacity to the nuclear thermal coefficient and the temporal variation of spin phase shift, the thermal power (P) absorbed from NIR irradiation in water was calculated as 0.092, 0.189, 0.255 and 0.354 W corresponding to incident laser power (P_0) of 1, 2, 3 and 4 W, respectively. The experimental SAR was measured as 18.43, 37.85, 51.00 and 70.86 W kg^{-1} corresponding to SIR of 200.36, 400.72, 601.10 and 801.44 W kg^{-1}, respectively. The ratios of these figures correspond to absorptance (A) of 0.0920, 0.0945, 0.0849 and 0.0884, respectively. A linear regression of spatially averaged SAR vs. SIR in the center of the calorimeter cell yielded a line with a slope of 0.0851 for the absorption of the incident laser through a 5 cm beam path. This is a reasonable figure for A given the precision of the nuclear spin phase shift. The fraction of power absorbed through a 5 cm beam path was calculated as 0.0934 using the extinction coefficient and the linear absorption

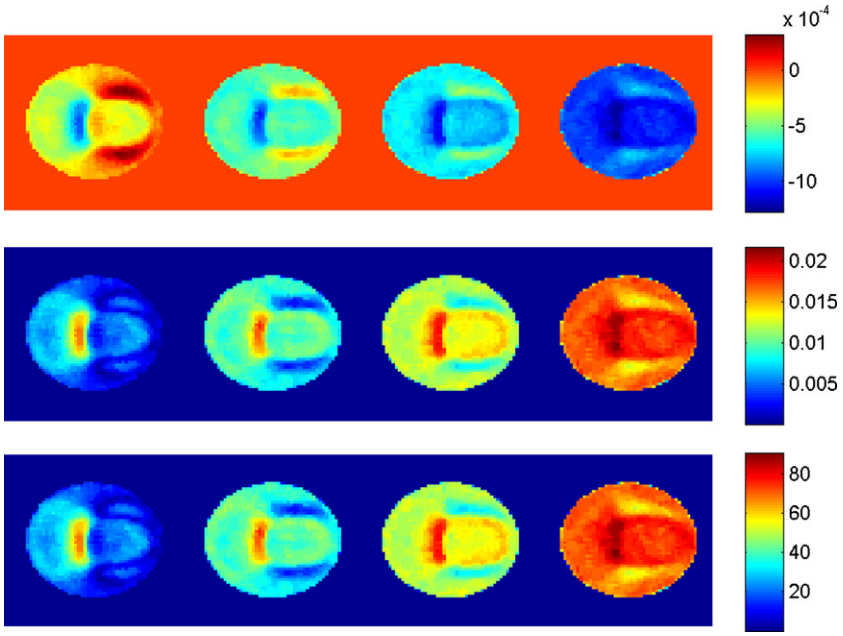

Fig. 4. Experimental $\dot{\phi}$, $\dot{\phi}/\phi_T$ and $c_p\dot{\phi}/\phi_T$ (top, middle and bottom rows) averaged over 12 min for a water sample irradiated by a NIR laser beam with power levels of 1, 2, 3 and 4 W (left to right columns), respectively.

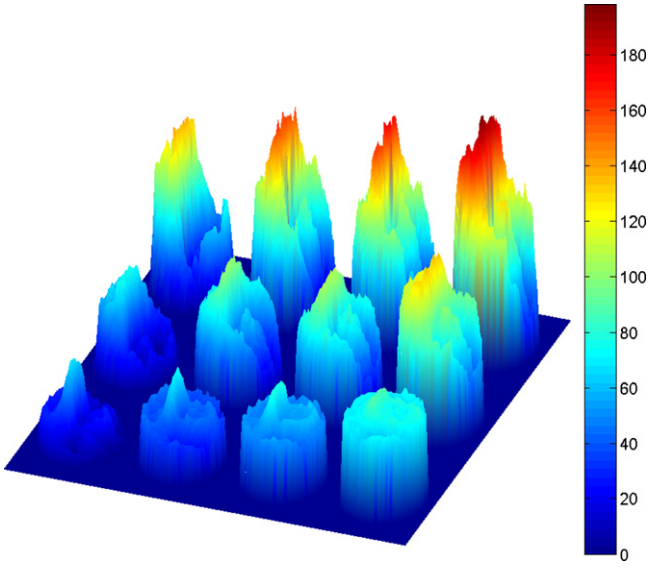

Fig. 5. Experimental SAR averaged over 5, 10 and 12 min (bottom to top) in water irradiated by NIR laser at power levels of 1, 2, 3 and 4 W (left to right). SAR was measured in a 3 mm axial imaging slice (0.3 g of water) in the center of a cylindrical cell irradiated along the axis through a fiberoptic.

coefficient ($\alpha = 0.0196\,\text{cm}^{-1}$) for water at a wavelength of 810 nm [40]. The absorption of light through 1 cm beam path in water at the wavelength of 810 nm was measured as 0.042 using a UV–vis spectrophotometer.

In NMR imaging, SAR is shown to vary in homogeneous substances with radiofrequency and sample radius with maximum local SAR and heating taking place at the surface [41]. The power deposition in NMR is discontinuous and depends on the substance and pulse parameters such as pulse power, duty cycle, etc. The average RF power using a single shot RARE sequence with 128 refocusing pulses, a pulse power of 2.5 W, a pulse width of 2 ms and a pulse sequence repetition time of 23 s was estimated to be 0.0275 W corresponding to SIR of 5.5 W kg^{-1} for 5 g water sample. A measurement of a single slice (3 mm) in the center of the cell showed a local SAR value of 0.8 W kg^{-1} (averaged over 12 min and 0.3 g of water). Although, the absorptance can be measured by this thermal method for a continuous wave radiation, it is much more complicated for a pulse radiation as in NMR pulse sequences. However, an average absorptance may be used to estimate the fraction of average incident RF power absorbed in the water sample ($A = 0.14$) in this experimental configuration.

A spatial resolution of 0.273–0.5 mm per pixel or 0.224–1 mm^3 per voxel, a temporal resolution of 11.5 s in imaging, acquisition times of 0.06–1.28 s for relaxation rates and equilibrium nuclear magnetization, and 2.0 s for nuclear shielding were used in spectroscopic measurements. These resolutions were adequate given the

Table 6
Experimental SAR measurements averaged over 12 min and 0.3 g of water subjected to three sources of power, RF, NIR and Thermal, at a 2 T magnet.

Power source	P [W]	$\dot{\phi}$ [rads s^{-1}]	$\frac{\dot{\phi}}{\phi_T}$ [K s^{-1}]	$c_p\frac{\dot{\phi}}{\phi_T}$ [W kg^{-1}]
RF	0.0275	-1.1434×10^{-5}	1.9430×10^{-4}	0.8005
NIR	0.5	-1.3302×10^{-4}	2.2604×10^{-3}	9.3128
NIR	1.0	-2.5905×10^{-4}	0.4402×10^{-2}	18.4263
NIR	2.0	-5.3211×10^{-4}	0.9042×10^{-2}	37.8487
NIR	3.0	-7.1704×10^{-4}	1.2184×10^{-2}	51.0032
NIR	4.0	-9.9624×10^{-4}	1.6929×10^{-2}	70.8627
Thermal	0.08	-1.4858×10^{-4}	2.5247×10^{-3}	10.5685
Thermal	0.16	-3.0149×10^{-4}	5.1231×10^{-3}	21.4453
Thermal	0.24	-4.2891×10^{-4}	7.2882×10^{-3}	30.5084
Thermal	0.32	-5.0035×10^{-4}	8.5022×10^{-3}	35.5901

relatively low heating rates used in these experiments. However, much higher spatial and temporal resolution is possible in NMR imaging and spectroscopy. The spectroscopic and imaging measurements can be used in combination to meet the requirements for spatial and temporal resolution.

5. Conclusion

The feasibility of measuring the specific heat and specific absorption rate by NMR calorimetry has been demonstrated with three NMR parameters in three substances exhibiting distinct thermal and NMR properties. The feasibility of measuring the specific heat of liquids indicates that the NMR calorimetry may be applied to a wide range of different substances and materials. NMR calorimetry can be used to measure the specific absorption rate directly and non-invasively in substances subjected to electromagnetic irradiation. NMR calorimetry may also be used to measure the specific heat and specific absorption rate of biological substances and tissues which are important factors in physiology and medicine.

References

[1] P.J. Haines, Royal Society of Chemistry (Great Britain), Principles of Thermal Analysis and Calorimetry, Royal Society of Chemistry, Cambridge, 2002.
[2] B. Wunderlich, Thermal Analysis, Academic Press, Boston, 1990.
[3] E.A. Turi, Thermal Characterization of Polymeric Materials, 2nd ed., Academic Press, San Diego, 1997.
[4] G. Kaletunç, Calorimetry in Food Processing: Analysis and Design of Food Systems, Wiley-Blackwell, Ames, IA, 2009.
[5] N.J. Coleman, D.Q.M. Craig, Int. J. Pharm. 135 (1996) 13.
[6] G.E. Plum, K.J. Breslauer, Curr. Opin. Struct. Biol. 5 (1995) 682.
[7] H.B. Callen, Thermodynamics and An Introduction to Thermostatistics, 2nd ed., Wiley, New York, 1985.
[8] W.J. Smothers, Y. Chiang, Handbook of Differential Thermal Analysis, Chemical Pub. Co., New York, 1966.
[9] E.S. Watson, J. Justin, N. Brenner, M.J. Oneill, Anal. Chem. 36 (1964) 1233.
[10] P.S. Gill, S.R. Sauerbrunn, M. Reading, J. Therm. Anal. 40 (1993) 931.
[11] M. Reading, A. Luget, R. Wilson, Thermochim. Acta 238 (1994) 295.
[12] E. Gmelin, Thermochim. Acta 305 (1997) 1.
[13] B. Wunderlich, Thermochim. Acta 355 (2000) 43.
[14] B. Wunderlich, J. Therm. Anal. Calorim. 78 (2004) 7.
[15] D.H. Gultekin, J.C. Gore, 9th International Congress on Hyperthermic Oncology, St. Louis, MO, USA, 2004, p. 141.
[16] P.A. Bottomley, E.R. Andrew, Phys. Med. Biol. 23 (1978) 630.
[17] C.M. Collins, W. Liu, J. Wang, R. Gruetter, J.T. Vaughan, K. Ugurbil, M.B. Smith, J. Magn. Reson. Imaging 19 (2004) 650.
[18] J.W. Hand, R.W. Lau, J.J. Lagendijk, J. Ling, M. Burl, I.R. Young, Magn. Reson. Med. 42 (1999) 183.
[19] H. Cline, R. Mallozzi, Z. Li, G. McKinnon, W. Barber, Magn. Reson. Med. 51 (2004) 1129.
[20] US Federal Communications Commission, Consumer and Govermental Affairs Bureau, Cellular Telephone Specific Absorption Rate (SAR), 2010 (accessed 02/13/2010) http://www.fcc.gov/cgb/sar/.
[21] International Electrotechnical Commission, IEC 62209-1: Procedure to Determine the Specific Absorption Rate (SAR) for Hand-held Devices Used in Close Proximity to the Ear (frequency range 300 MHz to 3 GHz), Geneva, Switzerland, 2005.
[22] US Food and Drug Administration, Center for Devices and Radiological Health, Guidance for Industry and FDA Staff: Criteria for Significant Risk Investigations of Magnetic Resonance Diagnostic Devices, 2010 (accessed 02/13/2010) http://www.fda.gov/MedicalDevices/DeviceRegulationandGuidance/GuidanceDocuments/ucm072686.htm.
[23] International Electrotechnical Commission, Medical electrical equipment, IEC 60601-2-33: Particular Requirements for The Safety of Magnetic Resonance Equipment for Medical Diagnosis, Geneva, Switzerland, 2002.
[24] ICNIRP, Health Phys. 87 (2004) 197.
[25] W.E. Lamb, Phys. Rev. 60 (1941) 817.
[26] N.F. Ramsey, Phys. Rev. 78 (1950) 699.
[27] U. Liddel, N.F. Ramsey, J. Chem. Phys. 19 (1951) 1608.
[28] J.C. Hindman, J. Chem. Phys. 44 (1966) 4582.
[29] F. Bloch, Phys. Rev. 70 (1946) 460.
[30] N. Bloembergen, E.M. Purcell, R.V. Pound, Phys. Rev. 73 (1948) 679.
[31] P. Curie, Thèse – Faculté des sciences de Paris, Gauthier-Villars et fils, 1895.
[32] P. Langevin, Centre national de la recherche scientifique (France) Œuvres scientifiques de Paul Langevin, Centre national de la recherche scientifique, Paris, 1950.
[33] A. Abragam, The Principles of Nuclear Magnetism, Clarendon Press, Oxford, 1961.
[34] D.H. Gultekin, J.C. Gore, J. Magn. Reson. 172 (2005) 133.
[35] D.H. Gultekin, Ph.D. Thesis, Yale University, 2002.
[36] H.Y. Carr, E.M. Purcell, Phys. Rev. 94 (1954) 630.
[37] S. Meiboom, D. Gill, Rev. Sci. Instrum. 29 (1958) 688.
[38] A. Haase, J. Frahm, D. Matthaei, W. Hanicke, K.D. Merboldt, J. Magn. Reson. 67 (1986) 258.
[39] J. Hennig, A. Nauerth, H. Friedburg, Magn. Reson. Med. 3 (1986) 823.
[40] G.M. Hale, M.R. Querry, Appl. Opt. 12 (1973) 555.
[41] P.A. Bottomley, W.A. Edelstein, Med. Phys. 8 (1981) 510.